Field Imaging near to the surface of terahertz reflective optics using a vector network analyzer

MARYAM HAJJI*, JONATHAN HAMMLER, DAGOU ZEZE, CLAUDIO BALOCCO, AND ANDREW J GALLANT

Department of Engineering, Durham University, South Rd, Durham, DH1 3LE, UK.
**Corresponding author: maryam.hajji@durham.ac.uk*

A Vector Network Analyzer-based quasi-optical measurement system, which is suitable for mapping electric field intensity and phase near to the surface of terahertz reflective optics, is presented. The system uses a fixed five parabolic mirror and transmitter/receiver head arrangement which has the benefit of requiring only the sample to be swept during measurement. The system has been tested with a micromilled aluminum zone plate reflector used as an exemplar structure. The measured focal point of the zone plate reflector, at its designed frequency of 1 THz, is shown to correspond well to both Finite Difference Time Domain simulations and analytical theory. © 2017 Optical Society of America

***OCIS codes**: (300.6495) Spectroscopy, terahertz; (050.1970) Diffractive optics; (120.5700) Reflection; (160.3900) Metals; (160.4760) optical properties; (050.5080) phase shift.*

1. INTRODUCTION

The now traditional terahertz time domain spectroscopy (TDS) arrangement which typically relies on femtosecond laser excitation of a photoconductive source to generate a broadband pulse of terahertz radiation has become the mainstay system for measurements in this region. Coherent detection, used in the TDS configuration, leads to excellent signal to noise but the combination of both laser and terahertz beam alignment can make it difficult to extract reliable, reproducible electric field and phase information over long measurement runs. Laser beam drift affects both the emitter and receiver performance, introduces a time-varying systematic error that is difficult to remove and leads to unwanted peak signal and bandwidth variation [1].

A THz Vector Network Analyzer (VNA), which relies on a microwave (GHz) source that is frequency multiplied into the terahertz region, eliminates the need for laser alignment and removes concerns about beam drift. The terahertz radiation emerges from and is received by horn antennas which are mechanically coupled to waveguides. The frequency upmixing process is described in detail in [2], where measurements of achievable dynamic range are reported as approximately 90 dB, within a rectangular waveguide. The systematic errors introduced by the inclusion of antennas, beam steering mirrors and propagation through the ambient environment have been shown to be negligible by the sensitivity analysis performed in [3]. Following an appropriate calibration procedure, the typical precision of measured scattering- (S-) parameters (complex transmission and reflection) is ±1 %. Work is ongoing in comparing the system performance of terahertz-TDS and VNA systems in order to establish full interoperability [4].

The stable nature of the network analyzer's oscillators is well suited for the measurement and characterization of narrowband devices. Measuring directly in the frequency domain provides the ability to rapidly acquire many single-frequency measurements to increase SNR, or to investigate time-variant effects with a continuous wave (CW) source.

There is a need for light, compact and rugged optics to be incorporated into portable terahertz systems with field applications that include the space sector [5]. These optical components are required to focus, beam shape and to realize devices such as reflectarrays. It is essential that reliable characterization techniques are developed to validate the performance. Ideally, these techniques need to fully reveal the phase and amplitude of the electromagnetic field in the proximity to the components. Direct analysis in the frequency domain is desirable for diffractive components such as zone plates. Source technologies such as Quantum Cascade Lasers offer excellent power [6] but suffer from limited frequency sweep range compared to a terahertz VNA and have yet to be implemented for use in the sub-terahertz region.

Diffractive optical elements such as lenses and mirrors have been developed for use in many areas of the electromagnetic spectrum ranging from microwave to visible light [7-12]. In particular, the use of a Fresnel zone plate (FZP) as a focusing element, which was first recognized by Soret in the late 19th century [13], has attracted attention in recent years. This is beneficial in the millimeter wave region where conventional dielectric lenses and reflective optics are typically bulky. Although binary FZPs are lossy compared to multilevel zone plates, due to higher diffraction orders, they are much easier to fabricate and are well suited to test the reported measurement system.

In the Ka-band (26.5 to 40 GHz), Karimkashi and Kishk reported on the focusing behavior of Soret FZP lenses in the near field region with target applications for remote sensing [14].
In 2016, Pan et al [15] characterized FZPs in the terahertz region, at 350 GHz, with the aim of improving the focusing properties and directionality. They proposed a square grooved dielectric (PTFE) lens where the conventional concentric circular rings grooves found in a Soret FZP are replaced with square annuli. This was derived from a diagonal horn antenna and for use in terahertz wireless communication systems.
For reconfigurable structures, various groups have explored the use of optically tuned FZPs which rely on the photoexcitation of carriers in silicon to produce spatially varying electron plasma. This produces the metallic/dielectric variation required for an FZP shape but can be tuned by changing the light pattern which is used to illuminate the semiconductor. Such configurations have been experimentally studied in a transmission configuration. However, the tunability comes at the expense of requiring additional optical components to manipulate the nonterahertz beam [16-18].
When used as reflective components, FZPs can be fabricated from metals. Headland et al [19] recently reported the development of 3D printed metal zone plate. They characterized focal spot and beam shape using a terahertz-TDS system; with the highest reflective efficiency recorded at 530 GHz limited by the surface roughness and surface oxide due to the 3D printing process and use a titanium alloy respectively.
Here we report on the use of a terahertz VNA for the measurement and mapping of electric field intensity and phase near to the surface of reflective terahertz components. A fixed five parabolic mirror and transmitter/receiver head arrangement is presented which has the advantage of requiring only the sample to be swept during measurement. A micromilled aluminum FZP reflector structure has been fabricated as an exemplar structure. It uses a binary design which, although lossy compared to multilevel zone operating at 1THz plates (due to higher diffraTction orders), is easier to fabricate and is well suited to test the measurement system. Finite difference time domain (FDTD) simulations are used to support the experimental results presented in this work.

2. DESIGN AND SIMULATIONS

As a model component, we have fabricated a zone plate reflector based on the traditional Fresnel design [see Fig. 1a]. Manufacturing has been carried out using a bespoke micromilling system on an aluminum substrate [Fig. 1(b)] leading to a cost-effective, compact and light design.

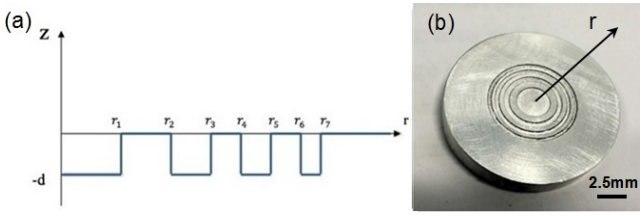

Fig. 1 (a) Schematic profile of FZPR with 4 zones (b) photograph of aluminum FZPR. The radial dimensions have been obtained from equation (1) given in the main text.

Figure 1(a) shows the configuration of the FZP reflector (FZPR) which consists of a set of concentric milled grooved zones. The Fresnel zone radii are periodic in r^2 with a period in r_p^2. The m^{th} zone radius, r_m is determined by

$$r_m^2 = mr_p^2 \quad \textbf{(1)}$$

The incoming beam is diffracted by the Fresnel zones interfering constructively at multiple focal points on the main optical axis with the first focal point located at [20]

$$F = \frac{r_p^2}{\lambda} \quad \textbf{(2)}$$

where F is the distance from the reflector and λ is the wavelength of interest. The reflector contains of four zones with a 13mm overall diameter, r_p =2.5 mm. This corresponds to a first focal point centered at 20 mm (for 1 THz). The numerical aperture (NA) for this configuration is 0.357. This structure offers the potential to choose a trade-off between resolution and depth of field and, with a low NA, the bias here is towards a longer depth of field. A nominal zone depth of 75 μm has been micromilled to produce the necessary π phase shift. The final fabricated structures had a measured zone depth of 62 μm with a 2.3 μm rms surface roughness at the bottom of each milled zone (compared to 0.32 μm in the unmilled area). It should be noted that this surface roughness is two orders of magnitude smaller than the free space wavelength at 1 THz. Therefore, it is reasonable to neglect its effect on the optical performance of the reflector.
A commercial 3D FDTD solver (Lumerical) has been used to simulate the effect of the zone plate reflector on an incident 1 THz frequency plane wave. The reflectors have been simulated using the same dimensions as the micromilled devices and within the same frequency range as the terahertz VNA operates. In the simulations, aluminum is assumed to be a perfect electrical conductor. Reflections are minimized through the use of a perfectly matched layer (PML) [21] located along the two boundaries perpendicular to the reflector axis. Periodic boundary conditions have been imposed on the sides of the reflector (i.e. equivalent to simulating a reflector array). This permits the simulation of plane wave. Figure 2(a) shows the electric field intensity on a plane perpendicular to the reflector at 1 THz and the electric field intensity along the main optical axis. As is also evident in the optical axis profile [Fig. 2(b)], the simulated electric field intensity FWHM in the region of the first focal point is spread between 15 and 25 mm; with a plateau at 20 mm. At Z = 6 mm, there is evidence of a higher order focal point. This is to be expected with the FZPR configuration which leads to higher order (closer to the reflector, but lower intensity) focal points. The simulated field intensity, plotted in the XY plane, for various Z distances from the reflector is shown in Fig. 3. It can be seen that by moving towards the focal point of reflector, the spot size becomes smaller and the electric field intensity has increased.

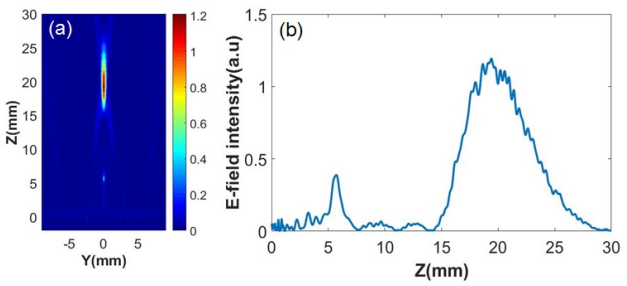

Fig. 2. FDTD simulated field intensity distribution in the (a) YZ plane (with X= 0 mm) and (b) along the optical, Z axis (with both X and Y= 0 mm).

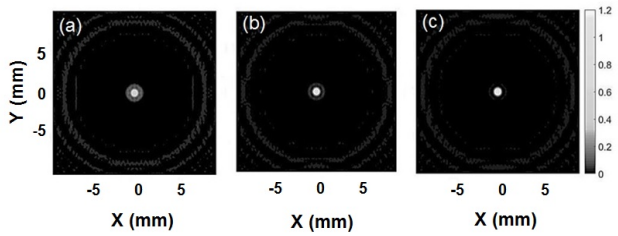

Fig. 3. FDTD simulated field intensity distribution in the XY plane at a distance, Z, along the optical axis, of (a) 19, (b) 20, (c) Z=21 mm from the reflector.

The simulated phase image at the focal point, Z = 20 mm, is shown in Fig. 4. The focal spot can be seen as a bright circular region of constructive interference (+π), flanked by an area of destructive interference (-π). A speckle pattern is superimposed on the simulation image; its shape arises from the use of periodic boundary conditions leading to interference from the adjacent reflectors. The effect of this interference can be minimized by using a larger simulation domain but at the expense of a much longer simulation time.

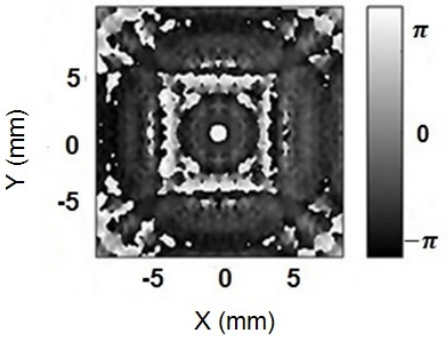

Fig. 4. Simulated phase image at 20 mm, showing the focal spot as a bright region of constructive interference (+π)

3. EXPERIMENT

The micro-milled aluminum reflector was tested with a terahertz-frequency VNA (Agilent Technologies N5224A PNA with Virginia Diodes WR1.0-VNAX frequency extension modules). The WR1.0-VNAX extension modules are the current state-of-the-art in mm-wave metrology systems and have an operating range from 0.75 to 1.1 THz. A WR1.0H diagonal horn antenna with an 11° divergence and horizontal polarization is coupled to each extension module waveguide [2]. Fig. 5 shows a schematic drawing of the experimental setup with the reflector mounted on a motorized XYZ optical stages. All components are rigidly mounted on an optical bench. This permits the measurement of XY scans with respect to the distance from the reflector, Z. The receiver detects the part of the reflected beam that is focused by the FZPR. Such scans allow a direct measurement comparison with the simulations presented previously. The alignment is carried out by using a white LED and diffuser screen at the receiver side and the transmission is maximized by fine alignment of the mirrors and beam splitter, while reducing the iris size.

The VNA measurement simultaneously provides information on both the amplitude and phase of the horizontally polarized electric field. The polarized radiation emerging from the horn antenna is collimated by off-axis parabolic mirror M5. This collimated beam is used to illuminate the Fresnel reflector through a silicon beam splitter which is set at a 45° angle with respect to the reflector's optical axis. The collimated beam illuminates all of the reflector and its surrounding region such that at maximum scan displacement the reflector is still fully illuminated. The electric field is imaged through an objective system, M1-3 and then focused by M4 to the receiver antenna. An iris is placed between M2 and M3 to minimize the effect of the scattered field and can influence the SNR. The distance from the origin on the Z axis is determined between the reflector and the focal point of M1 (as shown in Fig. 5). The uniformity of excitation is maintained because a fixed beam has been used and the sample moved. A key benefit of this configuration is that, by using fixed optics, the effect of parabolic mirrors and the beam splitter on the phase information during measurement is negligible.

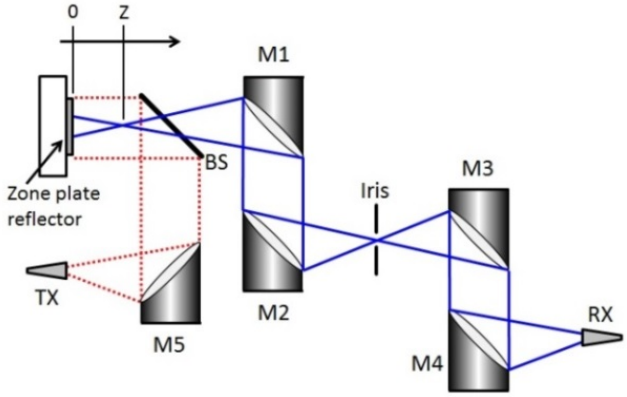

Fig. 5. Schematic diagram of the experimental setup with the reflector mounted as shown. All of the parabolic mirrors have a focal length of 10 cm.

The measured field intensity distributions, at 1 THz, in the XY plane are shown in Fig. 6 where the focal point is flanked by a dark ring structure resulting from destructive interference of the reflected beam. The round focal spots indicate low astigmatic aberrations. No smoothing or other post-processing has been applied to the images. There is good agreement between the simulated and measured results; although the measured central spot at the 20 mm focal point is slightly larger. The low numerical aperture of M1 limits the minimum resolvable feature size to 1.2 mm. However, there is a faint ring around the spot in the simulated image. This cannot be resolved by the measurement setup but will act to enlarge the measured spot. The outer bright ring in Fig. 6 relates to a reflection from the unpatterned aluminum area and also acts to confirm that illumination uniformity from M5 and the beam splitter is good.

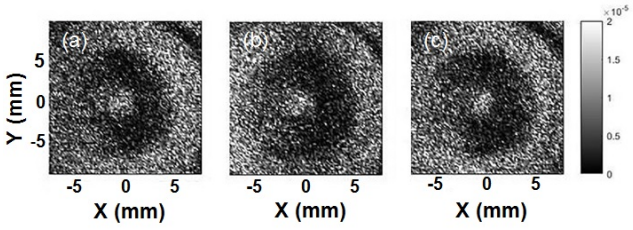

Fig. 6. The measured field intensity images, at 1 THz, for planes at (a) Z = 19 mm, (b) Z = 20 mm, (c) Z = 21 mm. All of the captured images are 100×100 pixels, corresponding to an area of 20× 20 mm.

The spot size at the focal point has been obtained from the FWHM of a Gaussian fit to the intensity profile. The fitting has been carried out using the least squares method. Fig. 7 shows the FWHM plot as a function of distance with respect to the reflector. As it can be seen, the smallest FWHM is observed at Z = 20 mm which corresponds to both the designed and simulated focal point. Here we report in the FWHM either side of the focal point which is also seen in field intensity distribution (Fig. 2). However, direct comparison between the simulated and measured FWHM away from focal point is not possible since the simulation displays very well-defined side lobes which prevent fitting with a Gaussian shape. Away from the focal point, the experimentally obtained FWHM plotted in Fig. 7 also factor in the effect of these side lobes.

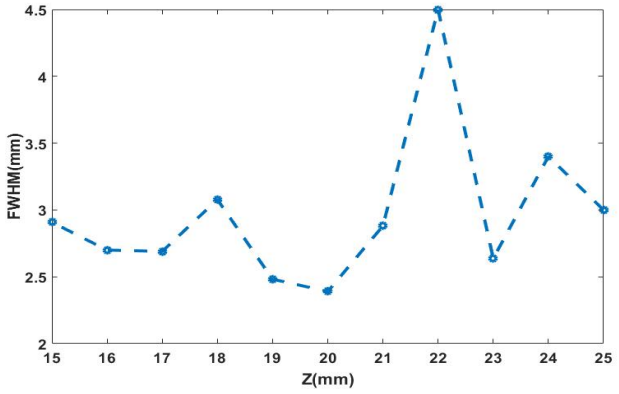

Fig. 7. FWHM of the measured focal point at distance, Z, from the reflector surface.

The experimental data is further supported by comparing the measured and simulated phase images, shown in Figs. 4 and 8 respectively. As explained earlier, the phase data is obtained simultaneously with the amplitude, and also therefore intensity, data during the XY scanning. The phase data is very sensitive to surface tilt which is readily observable as linear banding on the images. Surface tilt effects on the phase are minimized during the system alignment procedures. However, any remaining tilt is corrected via a software levelling approach. To do this, a linearly variable phase offset $\Delta\theta(x,y)$ is calculated using the following equation:

$$\Delta\theta(x,y) = \frac{2\pi}{\lambda} x \tan\alpha + \frac{2\pi}{\lambda} y \tan\beta, \qquad (3)$$

where α and β are the tilt angles of the reflector along the x and y direction, respectively. The value of phase is then wrapped between -π and π rad.

The levelled phase image shown in Fig. 8 clearly shows the transition from the focal spot, a region of constructive interference, to the surrounding circular region, with a lower field intensity formed by destructive interference.

The area of destructive interference in the measured phase image is smaller than in the simulation for two main reasons. First, as seen in the intensity images, the focal spot is larger than in the simulations which, in turn, enlarges the area of constructive interference in the phase images. Second, in the simulation, the area surrounding the focal spot includes an area of high contrast light and dark regions. However, as discussed earlier, the measurement system is resolution limited by the NA of mirror M1 (Fig. 5) and is unable to resolve such regions of high contrast in the phase images and instead is evident as a gradual grayscale transition from white to black. The bright area in the top right corner of the experimental phase image is a region of background reflection from the metallic substrate. To the left of the focal spot is a darker region, which is also evident in the intensity images (Fig. 6) as an area of higher intensity. This could be attributed to slight imperfection in the reflector manufacture (e.g. the surface is not completely flat).

The fundamental limits of the imaging system for both phase and amplitude are currently being studied with specific emphasis on a comparison with TDS systems. The ability to image the phase of the reflected beam in the region of the reflector surface could aid the design and characterization of next generation THz beam shaping devices, e.g. passive and active phased arrays. To open up techniques which are commonly used in the microwave field to the terahertz region, such as near field to far field transformation (or vice versa), details of both phase and amplitude are required.

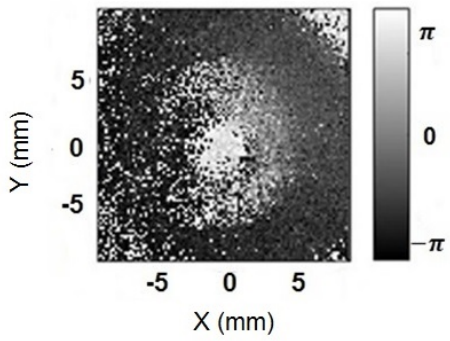

Fig. 8. Experimental phase image, at 1 THz, for Z = 20 mm.

4. CONCLUSIONS

In this paper, we have characterized a terahertz VNA-based quasi-optical configuration which can be used for electric field intensity and phase mapping as a function of distance from the surface of reflective optics. As an exemplar optical component, a zone plate reflector has been designed for operation at 1 THz and micromilled into aluminum. To obtain intensity and phase maps, the reflector was scanned in 3D space whilst the VNA extender heads and all other optical components were spatially fixed. The intensity and phase data has been compared with FDTD simulations and, in general, they showed good correspondence with the focal spot clearly visible and located at 20 mm away from the reflector surface. The reported setup permits the characterization of a wide range of beam shaping devices likely to provide light, compact and rugged optics necessary for incorporation into next generation terahertz systems. The raw data can be found at Dataset1.Ref.[22].

Funding Information. FP7 People: Marie Curie Actions (PEOPLE) (607521). NOTEDEV ITN, Engineering and Physical Sciences Research Council (EPSRC) (EP/M506321/1, EP/N021258/1).

References

1. W. Withayachumnankul and M. Naftaly, "Fundamental of measurement in terahertz time domain spectroscopy," J. Infrared, Millimeter, Terahertz, Waves **35**, 610-637(2014).

2. J. L. Hestler, Y. Duan, B. Foley, and T. W Crowe, "THz Vector Network Analyzer Measurements and Calibration," in *Proceedings of 21st International Symposium on Space Terahertz Technology*," (Oxford, 2010), pp.318-320.
3. J. Hammler, A. J. Gallant, and C. Balocco, "Free-Space permittivity measurement at terahertz frequencies with a vector network analyser," IEEE Trans. THz Sci. Technol. **6**, 817-823(2016).
4. M. Naftaly, G. C. Roland, D. A. Humphrey, and N. M. Ridler, "Metrology State-of-the Art and Challenges in Broadband Phase-Sensitive Terahertz Measurements, "in *Proceedings of the IEEE* 105 (2017), pp.1151-1165.
5. S. S. Dhillon, M. S. Vitiello, E. H. Linfield, A. G. Davies, M. C. Hoffmann, J. Booske, C. Paoloni, M. Gensch, P. Weightman, G. P. Williams, E. Castro-Camus, D. R. S. Cumming, F. Simoens, I. Escorcia-Carranza, J.Grant, S. Lucyszyn, M. Kuwata-Gonokami, K. Konishi, M. Koch, C.A .Schmuttenmaer, T.L. Cocker, R. Huber, A. G. Markelz, Z. D. Taylor, V. P. Wallace, J.A. Zeitler, J. Sibik, T. M. Korter, B. Ellison, S. Rea, P. Goldsmith, K. B. Cooper, R. Appleby, D. Pardo, P.G. Huggard, V.Krozer, H. Shams, M. Fice, C. Renaud, A. Seeds, A. Stöhr, M. Naftaly, N. Ridler, R. Clarke, J.E. Cunningham, and M. B. Johnston, "The 2017 terahertz science and technology roadmap," J. Phys. D **50**, 043001 (2017).
6. P. Dean, A. Valavanis, J. Keeley, K. Bertling, Y. L. Lim, R. Alhathlool, A.D. Burnett, L. H. Li, S.P. Khanna, D. Indjin, T. Taimre, A.D. Rakić, E.H. Linfield, and A.G. Davies "Terahertz imaging using quantum cascade lasers- a review of systems and applications," J. Phys. D:Appl.Phys **47,**374008(2014).
7. E.D. Walsby, R. Cheung, R. J. Blaikie, and D. R. Cumming, "Fabrication of multilevel silicon diffractive lenses for terahertz frequencies," Proc. SPIE **3879**, 79-87(1999).
8. S. Wang, T. Yuan, E.D. Walsby, R. J. Blaikie, S. M. Durbin, D. R. S. Cumming, J.Xu, and X.-C. Zhang, "Characterization of T-ray binary lenses," Opt.Lett **27**, 1183-1185(2002).
9. D. Feng, Y. Yan, G. Jin, and S. Fan, "Beam focusing characteristics of diffractive lenses with binary subwavelength structures," Opt. Commun. **239**, 345–352(2004).
10. M. Rachon, K. Liebert, A. Siemion, J. Bomba, A. Sobczyk, W. Knap, D. Coquillat, J. Suszek, and M. Sypek, "Geometrical Aberration Suppression for Large Aperture Sub-THz Lenses," J. Infrared, Millimeter, Terahertz Waves **38**, 347-355(2017).
11. A. Siemion, A. Siemion, J. Suszek, A. Kowalczyk, J. Bomba, A. Sobczyk, N. Palka, P. Zagrajek, A. Kolodziejczyk, and M. Sypek, "THz Beam Shaping Based on Paper Diffractive Optics," IEEE Trans. THz Sci. Technol. **6**, 568-575(2016).
12. W.D. Furlan, V. Ferrando, J. A. Monsoriu, P. Zagrajek, E. Czrewinska, and M. Szustakowski, "3D printed diffractive terahertz lenses," Opt. Lett. **41**, 1748-1751(2016).
13. J.L. Soret. "Ueber die durch Kreisgitter erzeugten Diffractionsphänomene," Ann. Phys. **232**, 99-113(1875).
14. S. Karimkashi, and A. A. Kishk, "Focusing properties of Fresnel zone plate lens antennas in the near- field region," IEEE Trans. Antennas Propag. **59**, 1481-1487(2011).
15. W. Pan, and W. Zeng, "Far-field characteristics of the square grooved-dielectrics lens antenna for the terahertz band," Appl. Opt. **55**, 7330-7336(2016).
16. S. Busch, B. Scherger, M. Scheller, and M. Koch, "Optically controlled terahertz beam steering and imaging," Opt.Lett.**37**, 1391-1393(2012).
17. C. Rizza, A. Ciattoni, L. Columbo, M. Brambilla, and F. Prati, "Terahertz optically tunable dielectric metamaterials without microfabrication," Opt.Lett.**38**, 1307-1309(2013).
18. X. Wang, Z. Xie, W. Sun, S. Feng, Y. Cui, J. Ye, and Y. Zhang, "Focusing and imaging of a virtual all-optical tunable terahertz Fresnel zone plate," Opt.Lett. **38**, 4731–4734(2013).
19. D. Headland, W. Withayachumnankul, M. Webb, H. Ebendorff-Heidepriem, A. Luiten, and D. Abbott, "Analysis of 3D-printed metal for rapid-prototyped reflective terahertz optics," Opt. Express **24**, 17384–17396(2016).
20. D. Attwood, "Soft X-Rays Microscopy with Diffractive Optics," in *Soft X-Rays and Extreme Ultraviolet Radiation: Principles and Applications* (Cambridge University Press, 1999), pp.337-394.
21. J. P. Berenger, *Perfectly Matched Layer (PML) for Computational Electromagnetics* (Morgan and Claypool, 2007).
22. The raw data can be found at http://doi.org/10.15128/r1vh53wv74p.